Journal of Alloys and Compounds 509 (2011) 6217–6221

Contents lists available at ScienceDirect

Journal of Alloys and Compounds

journal homepage: www.elsevier.com/locate/jallcom

Synthesis of MnO/C composites through a solid state reaction and their transformation into MnO_2 nanorods

Qin Hao [a], Liqiang Xu [a,*], Guangda Li [a], Zhicheng Ju [a], Changhui sun [a], Houyi Ma [a], Yitai Qian [a,b]

[a] Key Laboratory of Colloid and Interface Chemistry (Shandong University), Ministry of Education, Shanda nanlu 27, Jinan, Shandong 250100, PR China
[b] University of Science and Technology of China, Hefei, Anhui 230026, PR China

ARTICLE INFO

Article history:
Received 20 October 2010
Received in revised form 1 March 2011
Accepted 2 March 2011
Available online 10 March 2011

Keywords:
Composite materials
Oxide materials
Solid state reactions

ABSTRACT

MnO nanospheres encapsulated in carbon (MnO/C) composites were synthesized through a one-step solid state reaction between potassium permanganate and salicylic acid at 700 °C, which could be transformed into MnO_2 nanorods after being annealed in ambient atmosphere. Their formation mechanisms and electrochemical performances as anodes in Li-ion batteries (LIBs) were investigated. The first discharge capacity of MnO/C composites was 585.9 mA h g^{-1}, while that of MnO_2 was 1269 mA h g^{-1}, indicating their potential applications in LIBs.

1. Introduction

Manganese oxides, including MnO, MnO_2, Mn_2O_3, Mn_3O_4, Mn_5O_8, have been widely used as electrode materials, catalysts, and magnetic materials [1–4]. Among these, MnO plays an important role as the model system in the theoretical studies of the electronic and magnetic properties of rock salt oxides [5–7], and it is believed to be the promising anode material for lithium ion batteries (LIBs) [8]. Recently, MnO encapsulated in carbon core–shell like composites (MnO/C) have attracted increasing attention owing to their improved performances. There are some reports about the applications of MnO/C on the oxygen reduction reaction [9] and especially as anode material for LIBs. For example, the cell using MnO/C as anode electrode could deliver a capacity of 400 mA h g^{-1} at a rate of 400 mA g^{-1} [10]; the MnO/C nanorods had the capacity higher than 600 mA h g^{-1} during the first 40 cycles [11]; even the composites exhibited the capacity greater than 680 mA h g^{-1} at the 50th cycles [12]. However, the synthesis and property of MnO/C composites deserve more investigations.

MnO_2, as another manganese oxide, is extensively used on catalysis, ion-sieves, and supercapacitors [13–16]. It is also employed as reversible electrode material in LIBs [13,17–20]. Compared with graphite, MnO_2 always has higher capacities. For instance, Wu and Chiang reported that the capacity of the first cycle of MnO_2 nanowires was approximately 1160 mA h g^{-1} [21]. Moreover, the reversible capacity of MnO_2 interconnected nanowires could reach up to 800 mA h g^{-1}, which remained nearly constant even after 100 cycles [19]. Chen et al. also stated that the initial capacity of the as-prepared γ-MnO_2 hollow microspheres and nanocubes were 1071 and 1041 mA h g^{-1}, respectively [22]. Moreover, MnO_2/carbon nanotubes electrode exhibited a reversible capacity of 801 mA h g^{-1} without capacity fade for the first 20 cycles [23]. Therefore, MnO_2 is one of the most attractive anode materials in practice.

In this article, we presented a facile method to prepare MnO/C composites through a solid state reaction between salicylic acid (2-hydroxybenzoic acid) and potassium permanganate ($KMnO_4$). Moreover, MnO_2 nanorods were produced by simply annealing the composites in ambient atmosphere. Their formation mechanisms and electrochemical performances as anode materials in LIBs were also investigated.

2. Experimental

2.1. Preparation of MnO/C composites

In a typical experimental procedure, 1.0 g of salicylic acid and 1.0 g of $KMnO_4$ were added into a stainless-steel autoclave of 20 mL capacity. The autoclave was sealed and heated at 700 °C for 12 h in an electronic furnace. The precipitates in the autoclave were collected and washed with absolute ethanol, dilute hydrochloric acid and distilled water. After that, these products were dried in a vacuum at 60 °C for 5 h for further characterization.

2.2. Synthesis of MnO_2 nanorods

The as-obtained MnO/C was placed in a ceramic crucible, and then it was calcined from room temperature to 700 °C for 20 h in ambient atmosphere. Finally, the dark brown powders were collected.

* Corresponding author. Tel.: +86 531 88364543; fax: +86 531 88366280.
E-mail address: xulq@sdu.edu.cn (L. Xu).

0925-8388/$ – see front matter © 2011 Elsevier B.V. All rights reserved.
doi:10.1016/j.jallcom.2011.03.005

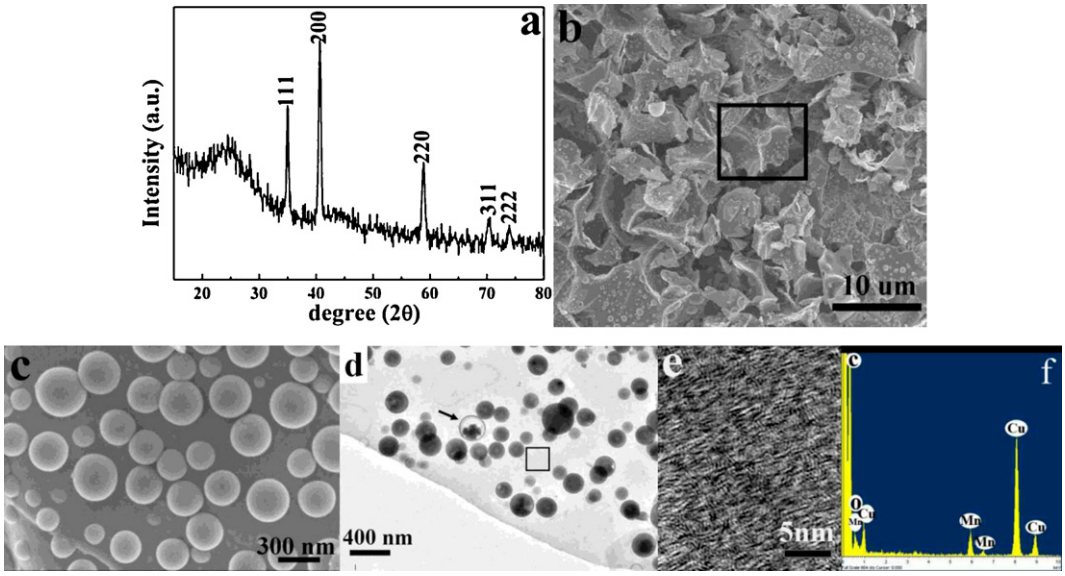

Fig. 1. (a) Typical XRD pattern, (b and c) SEM and (d) TEM images of the as-obtained MnO/C composites. (e) HRTEM image of the part marked with a black square frame and (f) the EDS of a randomly selected area arrowed in (d).

2.3. Characterization

The X-ray powder diffraction (XRD) patterns of the products were provided using a Bruker D8 advanced X-ray diffractometer equipped with graphite-monochromatized Cu Kα radiation (λ = 1.5418 Å). The morphology and structure of the samples were observed through the field emission scanning electron microscopy (FESEM, JEOL JSM-7600F), transmission electron microscope (TEM, H-7000) and high-resolution TEM (HRTEM, JEOL-2100). Thermal gravimetric analysis (TGA) was taken on a Mettler Toledo TGA-SDTA851 thermal analyzer apparatus under ambient atmosphere.

2.4. Electrochemical test

The anodes were prepared by mixing the MnO/C or MnO_2, acetylene black, and poly (vinyl difluoride) (PVDF) at a weight ratio of 80:10:10 or 75:15:10 in N-methyl pyrrolidone (NMP) into slurry. Then the mixture was rolled into a sheet, and the sheet was cut into circular strips of 8 mm in diameter. The strips were then dried at 100 °C for 12 h. Each cell typically contained about 3–5 mg of active material. Electrochemical test cell was assembled in argon-filled dry glove box using a lithium metal sheet as the counter electrode. A 1 M solution of $LiPF_6$ in ethylene carbonate, diethyl carbonate and ethyl methyl carbonate with the volume ratio of 1:1:1 was employed as the electrolyte. Celgard 2400 microporous polypropylene membrane was used as separator. The galvanostatic charge/discharge tests were performed within a Land CT2001 battery tester. The electrochemistry impedance spectroscopy (EIS) was measured on a Princeton Applied Research by applying an alternating current voltage of 10 mV in the frequency from 1 Hz to 100 kHz.

3. Results and discussion

The typical XRD pattern of the composites after being treated with HCl (Fig. 1a) shows that the sample is composed of two phases: the broad peaks with relatively lower intensity correspond to the diffraction of carbon; the rest five sharper peaks could be indexed as MnO (JCPDS card no. 07-0230). The SEM image (Fig. 1b) depicts that the sample is mainly consisted of curvy plates with some spheres interspersed on the surfaces, which are magnified in Fig. 1c. The HRTEM image (Fig. 1e) of the bald part framed in a square in Fig. 1d exhibits a disordered stacking feature, which indicates the plates are made up of amorphous carbon with low crystallinity. The EDS spectrum of a randomly selected sphere (Fig. 1f) indicates that chemical compositions of the sample are C, Mn, O and Cu (the Cu peaks originate from the copper grid that supports the specimen). Some spheres present core–shell structure with hollow inside, in which the MnO is partly eroded by HCl (such as the sphere arrowed in Fig. 1d). Therefore, the above results reveal that MnO spheres should be embedded in carbon plates.

The thermal stability of the as-prepared composites was studied by TGA in ambient atmosphere (Fig. 2a). It is found that the weight of the products did not change significantly below 350 °C.

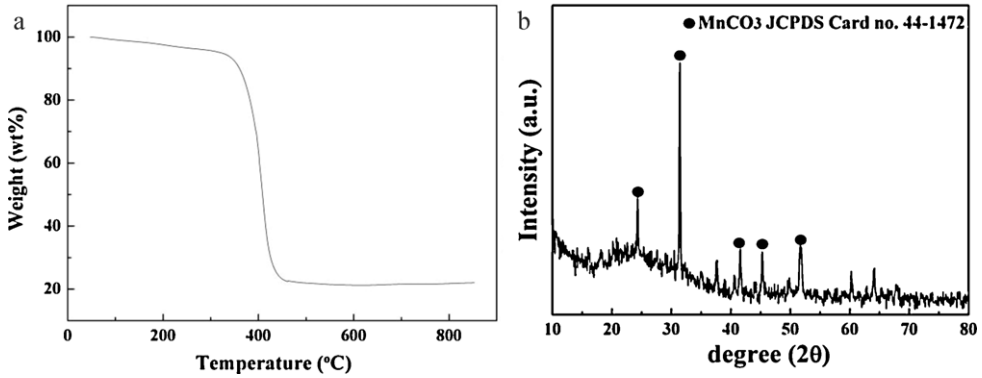

Fig. 2. (a) The thermal gravimetric curve of the MnO/C composites. (b) The XRD pattern of the product prepared at 400 °C.

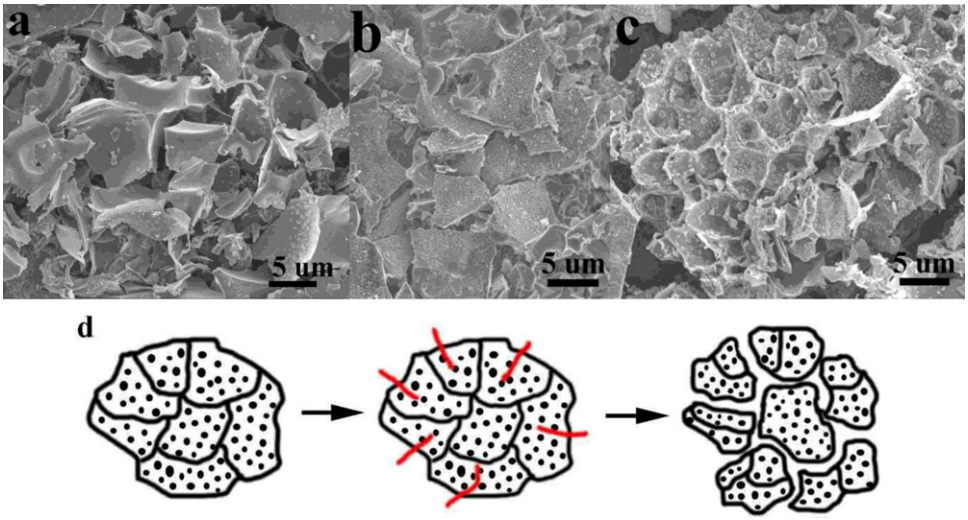

Fig. 3. SEM images of the product obtained at (a) 500 °C, (b) 600 °C for 12 h and (c) 700 °C for 3 h. (d) Schematic illustration of the mechanism for the formation of MnO/C curvy plates.

However, a distinct weight loss occurred within 350–450 °C, which was caused by the integrative effect of the weight loss (arising from the combustion of carbon to CO_2) and the weight gain (arising from the oxidation of MnO). Once the temperature exceeded 450 °C, the weight kept nearly constant.

There are functional groups (hydroxyl, carboxyl) on the benzene ring of salicylic acid (monohydroxybenzoic acid), both of which were reactive with $KMnO_4$ at high temperature. When benzoic acid or phenol was used instead of salicylic acid, irregular agglomerates were the main product. In addition, the heating temperature should be no lower than 400 °C, otherwise the major product would be $MnCO_3$ and unknown impurity (Fig. 2b). Therefore, MnO may originate from the decomposition of $MnCO_3$ at high temperature. There was no sign of other high-valence oxides being formed, which might be attributed to the existence of carbon with reducibility in the product [8]. Furthermore, the SEM images of the samples obtained at 500, 600 and 700 °C (corresponding to Figs. 3a and b and 1b, respectively) indicate that the proportion of the spheres on the plates increased as the temperature raised. Based on the above results, the quicker release of MnO may be the key factor causing this interesting structure. In order to further understand the formation process, TEM was used to record the morphology of the product after 3 h of reaction at 700 °C (Fig. 3c). The result manifested that some honeycomb-like products were produced co-existing with some uniform spheres on their surfaces. It is deduced that those ultimate curvy plates with spheres adhering to may be originated from the rupture of these honeycombs accompanying the prolonged reaction time at high temperature. The brief formation process of the curvy plates is described in Fig. 3d. At first, the MnO/C honeycombs were formed. Subsequently, the honeycombs splited along various directions as the reaction proceeded (referring to the red lines in Fig. 3d). (For interpretation of the references to colour in this text, the reader is referred to the web version of the article.) Eventually, as the division continued, adopting the crooked seam connecting the honeycomb internally, here came plenty of curvy plates which chiefly structured the product. This could refer to the plate framed in square in Fig. 1b.

Fig. 4a gives the XRD pattern of the product after annealing MnO/C composites at 700 °C for 20 h in ambient atmosphere, which can be indexed to a tetragonal phase [space group: I4/m (87)] of MnO_2 (JCPDS Card no. 44-0141), as the carbon and MnO in the composites were oxidized into CO_2 and MnO_2 due to the existence of O_2 in the air, respectively. The SEM image (Fig. 4b) presents that the sample is mainly composed of nanorods with diameters of 100–300 nm and length of ~2.5 μm. The HRTEM image of a randomly selected nanorod (Fig. 4c) shows the lattice spacing of 0.48 nm, which corresponds well to the (2 0 0) plane of MnO_2. In order to investigate the growth process of the nanorods, samples were exampled in detail at various stages of annealing process under TEM observation (Fig. 5a–c), which clearly exhibited the shape evolution of MnO_2 from particles to rods. After 3 h of the annealing process, the irregular particles were the main products, from which a few rods were extended (Fig. 5a), performing as the origin of the growth. When the annealing time reached 10 h, more nanorods formed with the consumption of the irregular particles, and the proportion of rods became higher and higher with prolonged annealing time (Fig. 5b). Once the reaction

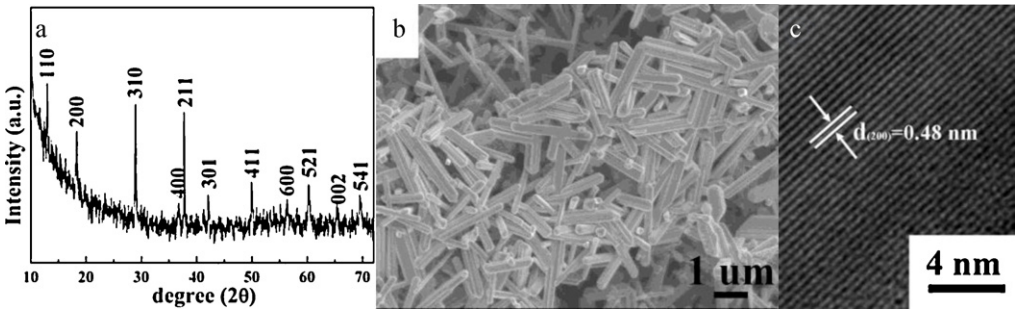

Fig. 4. (a) Typical XRD pattern, (b) SEM images and (c) HRTEM images of the obtained MnO_2 after the annealing process.

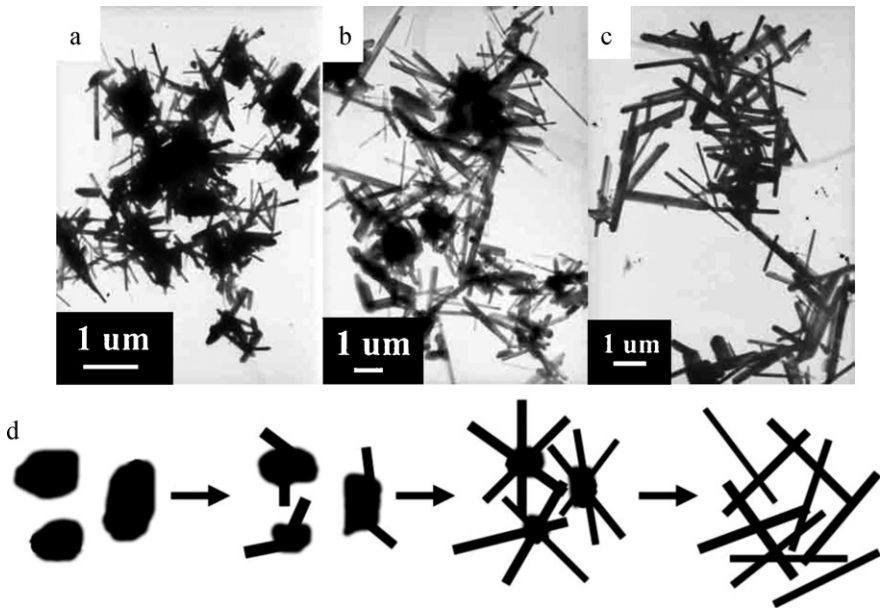

Fig. 5. TEM images of the product when the annealing time is (a) 3 h, (b) 10 h, (c) 20 h in ambient atmosphere and (d) the schematic illustration about the formation mechanism of MnO_2 nanorods.

time reached 20 h, the particles were exhausted and the regular nanorods were the predominant products (Fig. 5c). The growth process of MnO_2 nanorods can be described as follows. At first, the MnO may be deoxidized into manganese by the reductive carbon at high temperature. The as-produced metal of manganese would be subsequently oxidized into MnO_2 nanorods by the oxygen in air (see the schematic shown in Fig. 5d), the above growth process was similar with the previous reports about the synthesis of one dimensional metal oxides using carbon-assisted method, such as nanotubes and nanowires [24,25].

The performances of the as-prepared MnO/C and MnO_2 as anode materials in LIBs were tested. Fig. 6a and b present their first charge/discharge curves at the density of 25 and 150 mA g^{-1}, respectively. The initial discharge capacity of MnO/C composite was 585.9 mA h g^{-1}, which was lower than that of the 5 wt% carbon coated MnO anode (with particle size of ~30 nm and reversible capacity of 650 mA h g^{-1}) [10]. The reason may be their different content of carbon and particle sizes, because the electrochemical properties of the materials are influenced by their structure, morphologies, and composition. For example, smaller particle size can shorten the transportation/diffusion path for both of electrons and ions; higher surface area boosts the mutual connection between the active materials and electrolytes; porous or interconnective structure supply extra accessible space for lithium ions [26–28]. The initial discharge capacity of the as-prepared MnO_2 nanorods was 1269 mA h g^{-1}, which was equal to the previous reported MnO_2 materials, implying their potential applications in LIBs, but it remained ~500 mA h g^{-1} after 15 cycles (the capacity retention was ~40%). Therefore, there are spaces for further improvement of their cycling performances through tuning the morphologies, sizes or phases of the products [19,21,22], which deserves further investigations.

Fig. 7a and b shows the Nyquist impedance spectra of the batteries using MnO/C composites and MnO_2 as anodes before cycles, respectively. An intercept on the real axis Z_{re} at high frequency is attributed to the resistance of the electrolyte (R_e). The semicircle in the high-middle frequency region is assigned to the charge transfer resistance (R_{ct}), which is approximately equal to the numerical value of the diameter of the semicircle on the Z_{re} axis. The straight line in the low frequency region is associated with the diffusion of Li^+ into the bulk of the electrode material (Warburg impedance). The parameters of the equivalent circuit are recorded in Table 1,

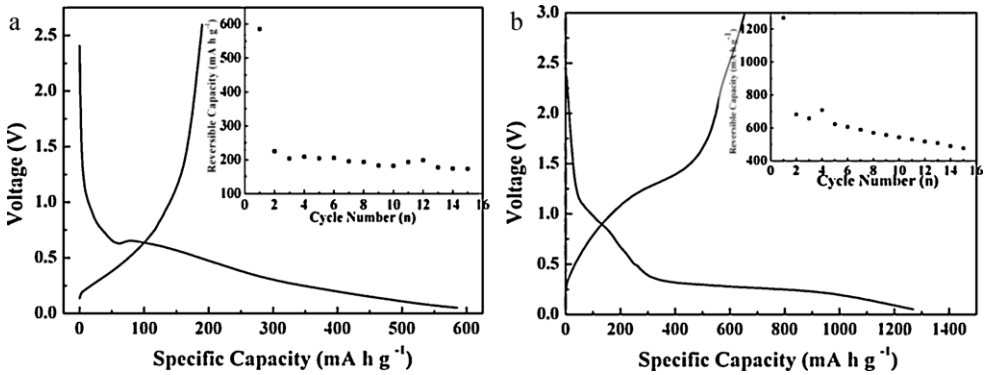

Fig. 6. The first discharge charge curves and cycling behavior for electrodes of (a) MnO/C composites and (b) MnO_2 nanorods vs Li/Li^+ at a constant current density of 25 and 150 mA g^{-1}, respectively.

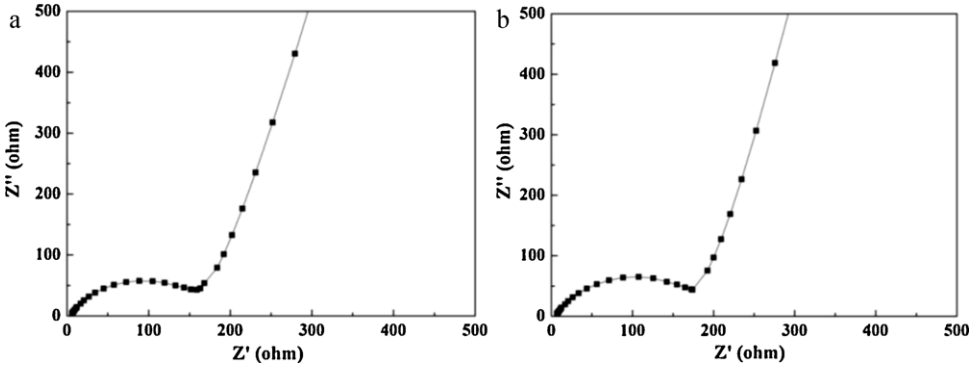

Fig. 7. Impedance spectra of the batteries using (a) C/MnO composites and (b) MnO_2 as anodes before cycle.

Table 1
Impedance parameters of the cells prepared from C/MnO composites and MnO_2 samples.

Sample	R_e (Ω)	R_{ct} (Ω)	σ_w (Ω cm^2 S$^{-0.5}$)	D (cm^2 s^{-1})	i° (mA cm^{-2})
C/MnO	4.49	170.4	307.8	6.03E-16	1.51E-4
MnO_2	5.18	188.4	272.1	7.72E-16	1.36E-4

which were approximately calculated by the following Eqs. (1)–(3) [29–31].

$$Z_{re} = R_e + R_{ct} + \sigma_w \omega^{-0.5} \quad (1)$$

$$D = 0.5\left(\frac{RT}{An^2F^2\sigma_w C}\right)^2 \quad (2)$$

$$i^\circ = \frac{RT}{nFR_{ct}} \quad (3)$$

(σ_w: Warburg impedance coefficient, ω: angular frequency in the low frequency region, D: diffusion coefficient, n: number of electron transfer in the reaction, R: the gas constant, T: the absolute temperature, F: Faraday's constant, A: the area of the electrode surface, C: molar concentration of Li^+ ions [32], and i°: exchange current density.)

4. Conclusions

The core–shell like composites of MnO nanospheres and carbon plates were synthesized via a one-pot solid state reaction, which can be converted into regular MnO_2 nanorods through a simple subsequent annealing process. Their growth mechanisms were discussed in detail and the electrochemical tests indicated their potential applications as anode materials in LIBs.

Acknowledgments

This work was supported by the National Nature Science Foundation of China (Grant Nos. 20871075 and 20971079), the 973 Project of China (No. 2011CB935901), the Independent Innovation Foundations of Shandong University (Nos. 2009TS017 and 2009JC019), and Graduate Independent Innovation Foundation of Shandong University (GIIFSDU).

References

[1] O. Giraldo, S.L. Brock, W.S. Willis, M. Marquez, S.L. Suib, J. Am. Chem. Soc. 122 (2000) 9330.
[2] H.E. Wang, Z.G. Lu, D. Qian, S.P. Fang, J.F. Zhang, J. Alloys Compd. 466 (2008) 250.
[3] L.Q. Mao, D. Zhang, T. Sotomura, K. Nakatsu, N. Koshiba, T. Ohsaka, Electrochim. Acta 48 (2003) 1015.
[4] M. Regulski, R. Przeniosło, I. Sosnowska, D. Hohlwein, R. Schneider, J. Alloys Compd. 362 (2004) 236.
[5] I.V. Solovyev, K. Terakura, Phys. Rev. B 58 (1998) 15496.
[6] S.K. Nayak, P. Jena, J. Am. Chem. Soc. 121 (1999) 644.
[7] G.H. Lee, S.H. Huh, J.W. Jeong, B.J. Choi, S.H. Kim, H.C. Ri, J. Am. Chem. Soc. 124 (2002) 12094.
[8] X.P. Fang, X. Lu, X.W. Guo, Y. Mao, Y.S. Hu, J.Z. Wang, Z.X. Wang, F. Wu, H.K. Liu, L.Q. Chen, Electrochem. Commun. 12 (2010) 1520.
[9] S. Shanmugam, A. Gedanken, J. Phys. Chem. B 110 (2006) 24486.
[10] K.F. Zhong, X. Xia, B. Zhang, H. Li, Z.X. Wang, L.Q. Chen, J. Power Sources 195 (2010) 3300.
[11] B. Sun, Z.X. Chen, H.S. Kim, H.J. Ahn, G.X. Wang, J. Power Sources 196 (2011) 3346.
[12] J. Liu, Q.M. Pan, Electrochem. Solid-State Lett. 13 (2010) A139.
[13] J.H. Cheng, G. Shao, H.J. Yu, J.J. Xu, J. Alloys Compd. 505 (2010) 163.
[14] C.H. Liang, C.S. Hwang, J. Alloys Compd. 500 (2010) 102.
[15] F. Teng, S. Santhanagopalan, Y. Wang, D.D. Meng, J. Alloys Compd. 499 (2010) 259.
[16] T. Tomko, R. Rajagopalan, M. Lanagan, H. Foley, J. Power Sources 196 (2011) 2380.
[17] M. Minakshi, K. Nallathamby, D. Mitchell, J. Alloys Compd. 479 (2009) 87.
[18] B.X. Li, G.X. Rong, Y. Xie, L.F. Huang, C.Q. Feng, Inorg. Chem. 45 (2006) 6404.
[19] M.S. Wu, P.C.J. Chiang, J.T. Lee, J.C. Lin, J. Phys. Chem. B 109 (2005) 23279.
[20] A.M. Hashem, H.M. Abuzeid, K. Nikolowski, H. Ehrenberg, J. Alloys Compd. 497 (2010) 300.
[21] M.S. Wu, P.C.J. Chiang, Electrochem. Commun. 8 (2006) 383.
[22] J.Z. Zhao, Z.L. Tao, J. Liang, J. Chen, Cryst. Growth Des. 8 (2008) 2799.
[23] H. Xia, M. Lai, L. Lu, J. Mater. Chem. 20 (2010) 6896.
[24] C.N.R. Rao, M. Natha, Dalton Trans. 1 (2003) 1.
[25] C.N.R. Rao, G. Gundiah, F.L. Deepak, A. Govindaraj, A.K. Cheetham, J. Mater. Chem. 14 (2004) 440.
[26] W.Y. Li, L.N. Xu, J. Chen, Adv. Funct. Mater. 15 (2005) 851.
[27] F. Jiao, K.M. Shaju, P.G. Bruce, Angew. Chem. Int. Ed. 44 (2005) 6550.
[28] F.Y. Cheng, Z.L. Tao, J. Liang, J. Chen, Chem. Mater. 20 (2008) 667.
[29] A.Y. Shenouda, H.K. Liu, J. Alloys Compd. 477 (2009) 498.
[30] A.Y. Shenouda, H.K. Liu, J. Power Sources 185 (2008) 1386.
[31] A.Y. Shenouda, H.K. Liu, J. Electrochem. Soc. 157 (2010) A1183.
[32] A.J. Bard, L.R. Faulkner, Electrochemical Methods, second ed., John Wiley & Sons, New York, 2001, p. 231.